J. Fluid Mech. (2013), *vol.* 717, *pp.* 643–669.
doi:10.1017/jfm.2012.603

Density difference-driven segregation in a dense granular flow

Anurag Tripathi and D. V. Khakhar†

Department of Chemical Engineering, Indian Institute of Technology Bombay,
Powai, Mumbai 400076, India

(Received 21 January 2012; revised 4 September 2012; accepted 3 December 2012;
first published online 1 February 2013)

We consider the segregation of spheres of equal size and different density flowing over an inclined plane, theoretically and computationally by means of distinct element method (DEM) simulations. In the first part of the work, we study the settling of a single higher-density particle in the flow of otherwise identical particles. We show that the motion of the high-density tracer particle can be understood in terms of the buoyancy and drag forces acting on it. The buoyancy force is given by Archimedes principle, with an effective volume associated with the particle, which depends upon the local packing fraction, ϕ. The buoyancy arises primarily from normal forces acting on the particle, and tangential forces have a negligible contribution. The drag force on a sphere of diameter d sinking with a velocity v in a granular medium of apparent viscosity η is given by a modified Stokes law, $F_d = c\pi\eta dv$. The coefficient (c) is found to decrease with packing fraction. In the second part of the work, we consider the case of binary granular mixtures of particles of the same size but differing in density. A continuum model for segregation is presented, based on the single-particle results. The number fraction profile for the heavy particles at equilibrium is obtained in terms of the effective temperature, defined by a fluctuation–dissipation relation. The model predicts the equilibrium number fraction profiles at different inclination angles and for different mass ratios of the particles, which match the DEM results very well. Finally, a complete model for the theoretical prediction of the flow and number fraction profiles for a mixture of particles of different density is presented, which combines the segregation model with a model for the rheology of mixtures. The model predictions agree quite well with the simulation results.

Key words: complex fluids, granular media, low-Reynolds-number flows

1. Introduction

The flow of granular materials is encountered in many geophysical situations and industrial applications (Duran 2000). Granular mixtures typically exhibit segregation, i.e. de-mixing while flowing (Drahun & Bridgwater 1983; Dolgunin & Ukolov 1995; Hirshfeld & Rapaport 1997; Khakhar, McCarthy & Ottino 1997, 1999; Dolgunin, Kudy & Ukolov 1998; Ottino & Khakhar 2000; Rapaport 2002; Khakhar, Orpe & Hajra 2003; Jain, Ottino & Lueptow 2005; Cisar, Umbanhowar & Ottino 2006) or when energized by vibration (Thomas 2000; Hsiau & Chen 2002; Felix & Thomas 2004; Yang 2006; Lim 2010; Tai, Hsiau & Kruelle 2010). This phenomenon is not

† Email address for correspondence: khakhar@iitb.ac.in

desirable in many industrial processes where proper mixing of the constituents is very important for product and process quality. Segregation in avalanches affects the total runout length as well as the formation of levees (Gray & Thornton 2005; Phillips *et al.* 2006; Linares-Guerrero, Goujon & Zenit 2007; Johnson *et al.* 2012). Thus, an understanding of segregation phenomena is of considerable importance. Segregation of granular mixtures may occur due to differences in one or more of the properties of the grains, such as size (Thomas 2000; Felix & Thomas 2004; Gray & Thornton 2005; Schröter *et al.* 2006; Godoy *et al.* 2008; Chung, Liaw & Ju 2009; Wiederseiner *et al.* 2011; Marks, Rognon & Einav 2012), density (Khakhar *et al.* 1997, 2003; Shi *et al.* 2007; Sanfratello & Fukushima 2008; Sarkar & Khakhar 2008), shape (Pollard & Henein 1989), inelasticity (Brito *et al.* 2008; Brito & Soto 2009), or surface roughness and friction (Srebro & Levine 2003; Ulrich, Schröter & Swinney 2007). However, the two most effective drivers of particle segregation are size differences and density differences. Though there are a few studies dealing with the coupled effect of size and density (Hill *et al.* 1999; Jain *et al.* 2005; Hajra & Khakhar 2011), typically the effects of these two properties are considered independently to gain a better understanding of the segregation process. We consider the case of segregation solely due to density differences and present a brief review of previous related studies below.

Experiments (Hsiau & Chen 2002; Yang 2006; Tai *et al.* 2010) as well as simulations (Yang 2006) for vibrated beds show that heavy particles, while starting from a completely segregated state, concentrate near the centres of convection rolls of the system. Mixtures with a larger density ratio are segregated more completely and the granular temperature of the heavy particles is found to be higher than that of the light particles. Shi *et al.* (2007) in their experimental study of vibrated mixtures found that the light particles tend to rise to the top, forming a pure layer, and the segregation order parameter, defined as the ratio of the height of the pure top layer to the height of the bed, is dependent only on the density ratio of the particles. Even horizontal vibrations of a bed with a bumpy bottom have been shown to cause density segregation as in the case of vertical vibrations (Lim 2010).

Rotating cylinder studies of particles of different density show the formation of a core region of high-density particles with the light particles concentrating at the periphery (Ristow 1994; Khakhar *et al.* 1997, 2003; Cisar *et al.* 2006; Pereira *et al.* 2011). Khakhar *et al.* (1997) have studied the radial segregation of binary mixtures of particles of different density using experiments and simulations along with a continuum theory based on a species balance equation in the flowing layer by balancing the convective flow (due to rotation) with diffusion and segregation fluxes. Recently Pereira *et al.* (2011) have investigated the assumptions of this theory in detail, using distinct element method (DEM) simulations, which were shown to be in good agreement with experimental results. Khakhar *et al.* (1999) used transport equations from the kinetic theory of mixtures for a mixture of nearly elastic smooth particles to analyse density segregation. They found very good agreement between theory and simulations for flow over an inclined plane for the case of frictionless particles. However, for the case of frictional particles, a good match between theory and simulations was obtained only if temperature was used as a fitting parameter. The value of the fitted temperature was found to be an order of magnitude higher than the granular temperature.

The results of Khakhar *et al.* (1999), discussed above, indicate the existence of another temperature more appropriate for dense granular flows. Theoretical (Berthier, Barrat & Kurchan 2000) and experimental (Song, Wang & Makse 2005) studies as well as simulations (Barrat & Berthier 2000; Berthier & Barrat 2002) have shown that

such an *effective temperature* can be defined by means of a fluctuation dissipation relation. Mehta & Edwards (1989) established the connection between segregation and compactivity, which has an equivalence to the effective temperature, as shown by Kurchan (2000) and Makse & Kurchan (2002). However, experimental evidence for the description of granular segregation in terms of the effective temperature for mixtures of particles of different density was provided only recently by Sarkar & Khakhar (2008). The authors follow an effective medium approach and provide an expression for a segregation flux. Balancing the segregation flux with the diffusional flux, an expression for the equilibrium number fraction profile of the heavy particles is given in terms of an effective temperature. An important component of this approach is the estimation of the drag force on a sedimenting particle.

Most studies of the drag force and mobility of spherical beads in a granular medium relate to large beads in static systems that are confined (Zhou, Advani & Wetzel 2005; Candelier & Dauchot 2009, 2010; Takehara, Fujimoto & Okumura 2010) or free to dilate (Wieghardt 1975; Zik, Stavans & Rabin 1992; Albert *et al.* 1999; Chehata, Zenit & Wassgren 2003; Pica Ciamarra *et al.* 2004; Geng & Behringer 2005). The drag force is found to be independent of the velocity (Albert *et al.* 1999; Zhou, Advani & Wetzel 2004, 2007; Costantino *et al.* 2011) for low velocities of the bead. Careful measurements, however, show a logarithmic dependence of the drag force on the velocity, for low velocities (Geng & Behringer 2005; Caballero-Robledo & Clement 2009; Candelier & Dauchot 2009, 2010). A linear variation of the drag force is found at higher speeds (Zik *et al.* 1992; Candelier & Dauchot 2009, 2010). Candelier & Dauchot (2009, 2010) found that motion of the bead in the medium causes reduction in the solids fraction in the vicinity of the particle.

The drag force on a particle in flowing granular materials has been studied to a lesser extent. The motion of tracer particles in slowly sheared annular systems was studied by Song *et al.* (2005). It was found that the drag force varies linearly with the speed even for low velocities. A quadratic dependence of the drag force on velocity was observed in simulations of dilute flows (Wassgren *et al.* 2003) and for horizontal dragging in confined two-dimensional (2D) systems at high velocities (Takehara *et al.* 2010). Considering the sedimentation of a single higher-mass but equal-size particle in a gravity-driven granular flow over an inclined plane, we have recently shown (Tripathi & Khakhar 2011*a*) that the drag force on a heavy particle in a flowing granular medium is given by a modified Stokes law.

Four primary approaches have been used to model granular segregation, most studies focusing on mixtures of different-size particles: kinetic sieving (Savage & Lun 1988), kinetic theory (Jenkins & Mancini 1989), single-particle motion (Khakhar *et al.* 1997) and partial stresses (Gray & Thornton 2005). Marks *et al.* (2012) have recently used DEM simulations to study the approach based on partial stresses. The current work uses the approach based on the motion of single particles.

Segregation results in changes in the local rheology and consequently the flow. The segregation flux also depends on the local rheology. Thus, the flow and segregation are coupled, and a complete description requires a rheological model for mixtures. We have recently proposed an extension of the viscoplastic model of Jop, Forterre & Pouliquen (2006) to the case of mixtures, which describes, quite well, the rheology of mixtures differing in both size and density (Tripathi & Khakhar 2011*b*).

In this work, we present a continuum model for flow and segregation of granular mixtures of equal-size particles with different densities. The model is based on a theory for the motion of a single particle in a dense flow, the assumptions of which are validated by comparison to results at a particle scale from DEM simulations of dense

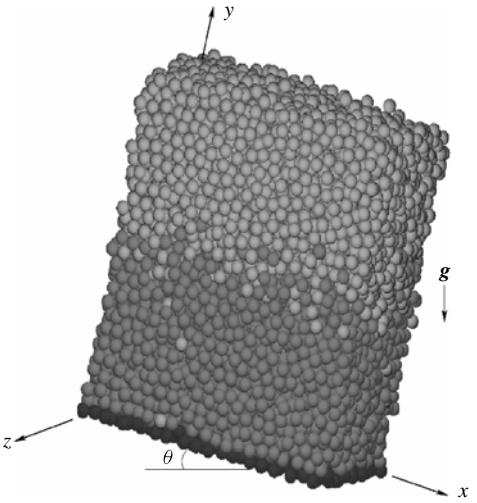

FIGURE 1. A typical snapshot of a mixture of particles flowing over an inclined plane at an inclination θ. A five-diameter wide slice of the system is shown. Dark grey spheres correspond to heavy particles and light grey spheres correspond to light particles. Black particles are the base, formed by taking a slice of thickness $1.2d$ from a random close-packed configuration of spheres of diameter d. The coordinate system used is shown along with the direction of gravity, $\boldsymbol{g}$.

granular flow on an inclined plane. The simulation method is described in § 2. The model formulation is presented in § 3 and results are presented in § 4. In that section, comparisons of model predictions to DEM simulations are done stage-wise. In the first part (§ 4.1), results for the motion of single particles are presented and compared to theory. In the second part (§ 4.2), the segregation model predictions are compared to DEM simulation results for mixtures; and in the third part (§ 4.3), the predictions of the combined segregation and flow model are compared to DEM simulations. The conclusions of the work are given in § 5.

2. Simulation methodology

We simulate slightly inelastic frictional spheres of diameter d flowing on a bumpy inclined surface, schematically depicted in figure 1. The simulation box is chosen to be $20d \times 20d$ long and wide in the x and z directions. The layer height in the y direction is $H = 25d$ for mixtures and $H = 20d$ for the tracer particle study. We use periodic boundary conditions in the flow (x) and the neutral (z) directions to simulate an infinitely long and wide chute without end or sidewall effects. The base is made rough by taking a slice of $1.2d$ thickness from a random close-packed configuration of spheres of size d. At the start of the simulation, the flowing particles are arranged with their centres on a cubic lattice with side $1.1d$, so that no two particles are in contact. Particles are given random initial velocities. The chute angle is kept sufficiently high ($\theta = 30^\circ$) for an initial period so that particles accelerate and gain energy. The inclination is then reduced to the desired value and the flow is allowed to achieve steady state.

For the tracer particle study, 16 particles, well separated from each other, in a slab of thickness d at a distance y from the base are selected from a layer of light particles

of mass m_L. The mass of these selected tracer particles is increased to a higher value m_H. The sinking velocities and the normal and tangential forces acting on the tracer particles in the y direction are noted at each step for a duration of time $t = 2\,(d/g)^{1/2}$ after discarding the data for an initial time $2\,(d/g)^{1/2}$, to avoid the effect of sudden change of mass of the tracer particles. For the case of mixtures, heavy particles (mass m_H) are placed initially in the upper half of the layer, while the light particles (mass m_L) are in the bottom half.

We follow a simulation method identical to that used by Tripathi & Khakhar (2011*b*) and model the individual particles as deformable soft spheres. A linear spring-and-dashpot type force scheme with static friction (Coulomb yield criterion) is employed in our simulations, which is identical to the L3 model of Silbert *et al.* (2001). The normal and tangential forces are calculated as the sum of an elastic spring force, which depends upon the deformation during a contact, and a viscous dashpot force, which depends upon the relative velocity of the contacting particles. Equations of motion for all the particles are integrated using a velocity-Verlet scheme with time step approximately equal to 1/50 of the binary collision time between two light particles for the values of parameters used in our simulations. The details of the simulation method can be found elsewhere (Tripathi & Khakhar 2011*b*).

The normal restitution coefficient is $e_n = 0.88$ and the tangential restitution coefficient $e_t = 1$. The value of the friction coefficient between the particles is $\mu_p = 0.5$. The stiffness of the particles in the normal direction is $k_n = 2 \times 10^5\, m_L g/d$ and that in the tangential direction is $k_t = 2k_n/7$. Measurements are taken only after the system has reached steady state, characterized by a constant kinetic energy and a time-invariant number fraction profile of heavy particles, in the case of mixtures. Results at steady state are obtained by calculating the properties of interest for 10 runs of 25 time units and averaging over four such sets. The time to reach steady state in the latter case when the initial condition has the heavy particles on top is $\sim 3000\,(d/g)^{1/2}$, due to the slow diffusion.

3. Theory

3.1. *Single particle motion*

Following Tripathi & Khakhar (2011*a*), we analyse the behaviour of a heavy tracer particle in a medium of light particles, which represents the simplest case of segregation due to density differences. We use an effective medium approach and assume the heavy tracer particle to be immersed in a continuum of density $\rho_m = \phi\rho_L$ (figure 2), where ϕ is the local packing fraction and ρ_L is the density of the light particles. The force on the tracer particle is

$$F_H = m_H g_y - F_b, \tag{3.1}$$

where $g_y = -g\cos\theta$ is the y component of the acceleration due to gravity and F_b is the buoyancy force exerted on the tracer particle by the granular medium. We use Archimedes principle to calculate the buoyancy force on the tracer particle, given by the weight of the fluid displaced by the tracer particle (Tripathi & Khakhar 2011*a*). To account for the presence of voids in the vicinity of the tracer particle, we assume that the tracer particle displaces a larger volume (shown as a dotted circle in figure 2) of the medium than its own volume, so that $F_b = \rho_L V_E g_y$, where V_E is the volume of the displaced medium.

The net force on the heavy tracer particle in the medium is

$$F_H = m_H g_y - \phi\rho_L V_E g_y. \tag{3.2}$$

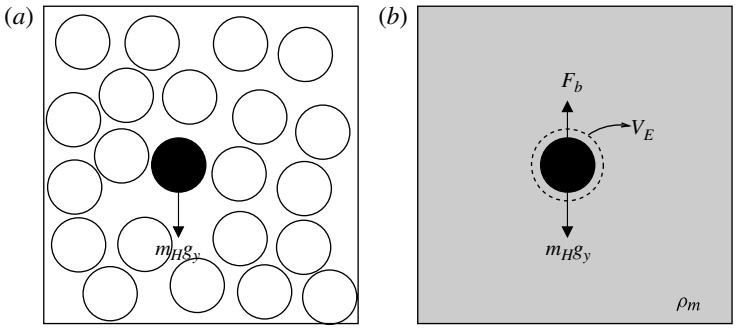

FIGURE 2. Schematic view of the system. (*a*) A heavy particle of mass m_H in a medium of light particles of mass m_L. (*b*) An effective medium view showing the buoyancy force F_b on the heavy particle of effective volume V_E.

The effective volume of a tracer particle V_E can be easily calculated as follows. For the case when the mass of the tracer particle is the same as that of the other particles, i.e. $m_H = m_L = \rho_L V$, there should be no net force on the tracer particle, i.e. $F_H = 0$, giving

$$V_E = V/\phi, \tag{3.3}$$

where V is the volume of the particle. Using this expression for V_E, the buoyancy force on the tracer particle in a granular medium of particles of mass m_L is

$$F_b = m_L g_y, \tag{3.4}$$

and the net force on the heavy tracer particle is

$$F_H = (m_H - m_L) g_y. \tag{3.5}$$

The effective volume accounts for the presence of voids around a tracer particle in the granular medium with each particle carrying some free volume with it. When the volumes of all the particles are equal, as in the present case, equation (3.3) shows that the effective volumes of all the particles are equal and every particle carries the same free volume with it. For the limiting case when the ratio of the volumes of the large to small particles is very large, the free volume carried by the large particle becomes vanishingly small, and the effective volume of the large particle becomes equal to the particle volume. In this limit, the usual Archimedes law is recovered.

The net force acting on the particle is in the negative y direction and causes the tracer particle to sink in the layer. The downward motion of the tracer particle is opposed by the viscous drag offered by the layer. In analogy to the Stokes drag force on a settling sphere in a fluid, we assume that the viscous drag force on the tracer particle is proportional to the viscosity (η) and settling velocity (v), i.e.

$$F_d = c\pi\eta d v, \tag{3.6}$$

c being a constant. At steady state, the net force on the tracer particle is balanced by the viscous drag force, i.e. $F_H = -F_d$, and using (3.5) and (3.6), we have

$$(m_H - m_L) g_y = -c\pi\eta v d. \tag{3.7}$$

Thus, at steady state, the theory predicts a linear relationship between the net force on the particle (left-hand side of the preceding equation) and ηv.

3.2. *Constitutive equations for density segregation*

We next extend our analysis to mixtures composed of particles differing in density following the approach of Sarkar & Khakhar (2008). The density ρ_m of the effective medium surrounding a heavy particle is now given by

$$\rho_m = \phi[f\rho_H + (1-f)\rho_L], \tag{3.8}$$

where $\rho_H = m_H/V$ is the density of heavy particles and $f = n_H/n$ is the number fraction of heavy particles, n_H being the number density of heavy particles and n the total number density. The buoyancy force acting on the heavy tracer particle, given as the weight of the displaced liquid, is then

$$F_b = \rho_m V_E g_y, \tag{3.9}$$

which upon simplification using (3.3) and (3.8) becomes

$$F_b = [fm_H + (1-f)m_L]g_y. \tag{3.10}$$

The net force on a heavy particle in the mixture is given by (3.1), which simplifies to

$$F_H = (1-f)(m_H - m_L)g_y. \tag{3.11}$$

In the above formulation, the only difference from the case of a single particle is the lower buoyancy due to the presence of heavy particles in the surrounding medium. At steady state, the sedimenting particle achieves a terminal velocity and $F_H = F_d$, which yields the segregation velocity of the heavy particle as

$$v_H = \frac{F_H}{\xi_H}, \tag{3.12}$$

where $\xi_H = c\pi\eta d$ is the *friction coefficient*, i.e. the inverse of the mobility (Berthier & Barrat 2002). We assume here that the Stokes law coefficient, c, is the same as for the tracer system. Since the Reynolds number is small, inertial effects are negligible and the mass of the particles should be unimportant in determining the drag force. For equal-size particles we note that the mobilities of the heavy and light particles are the same ($\xi_H = \xi_L$). Based on the segregation velocity obtained above, the segregation flux is given by

$$j^H = n_H(v_H - v_m), \tag{3.13}$$

where $v_m = fv_H + (1-f)v_L$ is the number average velocity in the y direction generated due to the segregation flux and $v_L = F_L/\xi_L$ is the segregation velocity of the light particles, with

$$F_L = f(m_L - m_H)g_y. \tag{3.14}$$

From the definitions of v_H and v_L we get $v_m = 0$, and the expression for the segregation flux becomes

$$j^H = nf(1-f)\frac{(m_H - m_L)g_y}{\xi_H}. \tag{3.15}$$

Note that the segregation flux (3.15) becomes zero in the case when the masses of the two species are equal ($m_H = m_L$) or when only one of the species is present ($f = 0$ or $f = 1$), as expected. A similar dependence on the composition has been found in a number of previous works for size segregation (Dolgunin & Ukolov 1995; Gray & Chugunov 2006; Marks *et al.* 2012) and for density segregation (Khakhar *et al.* 1997, 1999; Sarkar & Khakhar 2008).

We define an effective temperature using a fluctuation dissipation relation, the Einstein relation, as (Berthier & Barrat 2002; Song *et al.* 2005)

$$T_E = D_H \xi_H, \tag{3.16}$$

where D_H is the self-diffusivity of the heavy particles. The definition is based on an analogy with fluids for which the fluctuation dissipation relation is valid. Song *et al.* (2005) showed by means of experiments that the relation is also valid for a sheared packed bed of particles. In the present case, a minimal requirement for the validity of the concept is that the effective temperatures of the heavy and light particles are the same, which requires that $D_H = D_L$, where D_L is the self-diffusivity of the light particles. For diffusion over large length scales, the self-diffusivity in dense granular flows has been found to be dependent on particle diameter but independent of the mass of the particles (Sarkar & Khakhar 2008). Thus, $D_H = D_L$; this further implies that the self-diffusivities of the particles are equal to the binary diffusivity of the particles in the mixture (D).

Substituting for the effective temperature in (3.15), we obtain

$$j^H = nf(1-f)D\frac{(m_H - m_L)g_y}{T_E}. \tag{3.17}$$

The stress balance in the y direction yields

$$\frac{\mathrm{d}P}{\mathrm{d}y} = \rho_m g_y, \tag{3.18}$$

where P is pressure. Upon substitution of the above equation into (3.17) we obtain

$$j^H = nf(1-f)D\frac{(m_H - m_L)}{\rho_m T_E}\frac{\mathrm{d}P}{\mathrm{d}y}. \tag{3.19}$$

Thus the segregation in the present case is a consequence of the pressure gradient in the flow. Equation (3.19) is identical to the expression obtained from kinetic theory (Khakhar *et al.* 1999), but with T_E replaced by the granular temperature. The diffusion flux is given by

$$j^D = -nD\frac{\mathrm{d}f}{\mathrm{d}y}, \tag{3.20}$$

where D is the binary diffusivity of the particles. The constitutive equations given above can be used along with a transport equation of the form

$$\frac{\partial(nf)}{\partial t} = -\frac{\partial}{\partial y}(j^H + j^D), \tag{3.21}$$

to obtain the time-dependent concentration profile of the heavy particles, $f(y, t)$.

We note that it is straightforward to generalize the above equations to the 3D case. In this case, the different values of diffusivities in the three directions need to be taken into account.

3.3. *Flow and segregation in a layer at steady state*

As discussed in § 1, the segregation and the rheology of the mixture are coupled in a complex way. For a complete description of the flow, the momentum balance equations must be solved along with the segregation model and the rheological model.

Mass	m_L
Length	d
Time	$(d/g)^{1/2}$
Force	$m_L g$

TABLE 1. Definition of characteristic quantities used to make the variables dimensionless.

We consider the steady-state case here for the flow and segregation in the layer. At equilibrium, (3.21) yields,

$$j^H + j^D = 0, \tag{3.22}$$

assuming the base to be impenetrable. Using (3.17) and (3.20) in the above equation and rearranging gives the following equation for the equilibrium number fraction profile:

$$\frac{1}{f(1-f)}\frac{\mathrm{d}f}{\mathrm{d}y} = -\frac{(m_H - m_L)g\cos\theta}{T_E}. \tag{3.23}$$

Equation (3.23) indicates that the equilibrium profile depends only on the net force on a heavy particle and the effective temperature: a higher net force or a lower temperature will give a sharper profile and thus a greater extent of segregation.

Estimation of the effective temperature requires the viscosity (η) and the diffusivity (D). An expression for the viscosity is given below. For the diffusivity, we use the following scaling proposed by Savage (1993) for shear flows:

$$D = b\dot{\gamma}d^2, \tag{3.24}$$

where $\dot{\gamma}$ is the shear rate and b is a constant. Experimental measurements (Hajra & Khakhar 2005; Sarkar & Khakhar 2008) have shown the scaling to be valid for dense granular flows. We obtain the coefficient b from DEM simulations in § 4.2.

All the variables are non-dimensionalized using the characteristic mass, length, time and force given in table 1. Equations (3.4)–(3.7) in dimensionless form become

$$\bar{F}_b = \cos\theta, \tag{3.25}$$

$$\bar{F}_H = (\bar{m}_H - 1)\cos\theta, \tag{3.26}$$

$$\bar{F}_d = c\pi\bar{\eta}\bar{v}, \tag{3.27}$$

$$(\bar{m}_H - 1)\cos\theta = c\pi\bar{\eta}\bar{v}. \tag{3.28}$$

Similarly (3.23) in dimensionless form is given as

$$\frac{1}{f(1-f)}\frac{\mathrm{d}f}{\mathrm{d}\bar{y}} = -\frac{(\bar{m}_H - 1)\cos\theta}{\bar{T}_E}, \tag{3.29}$$

where

$$\bar{T}_E = c\pi\bar{\eta}\bar{D}, \tag{3.30}$$

with

$$\bar{D} = b\bar{\dot{\gamma}}. \tag{3.31}$$

In what follows, all the quantities reported are dimensionless and we omit the overbars.

For a steady flow over an inclined plane at an inclination θ, the balance and constitutive equations in dimensionless form are given below, following Tripathi & Khakhar (2011*b*). The shear stress τ_{xy} and the pressure P are given by

$$\tau_{xy} = -\sin\theta \int_y^H \phi\rho_{mix}\,\mathrm{d}y, \tag{3.32}$$

$$P = \cos\theta(1 - a\tan\theta)\int_y^H \phi\rho_{mix}\,\mathrm{d}y, \tag{3.33}$$

where ρ_{mix} is the local average density and a is a parameter that accounts for the anisotropy of the stress tensor due to non-zero normal stress differences (Tripathi & Khakhar 2011*b*). The packing fraction ϕ and local density ρ_{mix} are given by

$$\phi = \phi_{max} - (\phi_{max} - \phi_{min})I, \tag{3.34}$$

$$\rho_{mix} = \frac{fm_H + (1-f)}{V}, \tag{3.35}$$

where ϕ_{max} and ϕ_{min} are parameters of the model and I is the inertial number given as

$$I = \frac{\dot\gamma}{\sqrt{P/\rho_{mix}}}, \tag{3.36}$$

where $\dot\gamma = |\mathrm{d}v_x/\mathrm{d}y|$ is the shear rate. The shear stress and the pressure are related as

$$|\tau_{xy}| = \mu(I)P, \tag{3.37}$$

where $\mu(I)$ is the effective friction coefficient given as

$$\mu(I) = \mu_s + \frac{\mu_m - \mu_s}{I_0/I + 1}, \tag{3.38}$$

with μ_s, μ_m and I_0 being parameters of the model. The viscosity is defined as

$$\eta = \mu P/\dot\gamma = |\tau_{xy}|/\dot\gamma. \tag{3.39}$$

From (3.32) and (3.33), the effective friction coefficient at any inclination θ is

$$\mu = \frac{\tan\theta}{1 - a\tan\theta}. \tag{3.40}$$

Equations (3.38) and (3.40) can be combined to obtain the inertial number I as

$$I = I_0\left(\frac{\mu - \mu_s}{\mu_m - \mu}\right). \tag{3.41}$$

Using (3.36), the shear rate $\dot\gamma$ is given by

$$\dot\gamma = I\sqrt{\frac{P}{\rho_{mix}}}, \tag{3.42}$$

and the velocity profile $v_x(y)$ is obtained by integrating the shear rate as

$$v_x(y) = v_{x0} + \int_0^y \dot\gamma\,\mathrm{d}y, \tag{3.43}$$

where v_{x0} is the slip velocity at the base. For a rough base $v_{x0} = 0$. The parameters of the mixture rheological model were obtained previously by fitting to DEM simulation results (Tripathi & Khakhar 2011*b*) and are given in table 2.

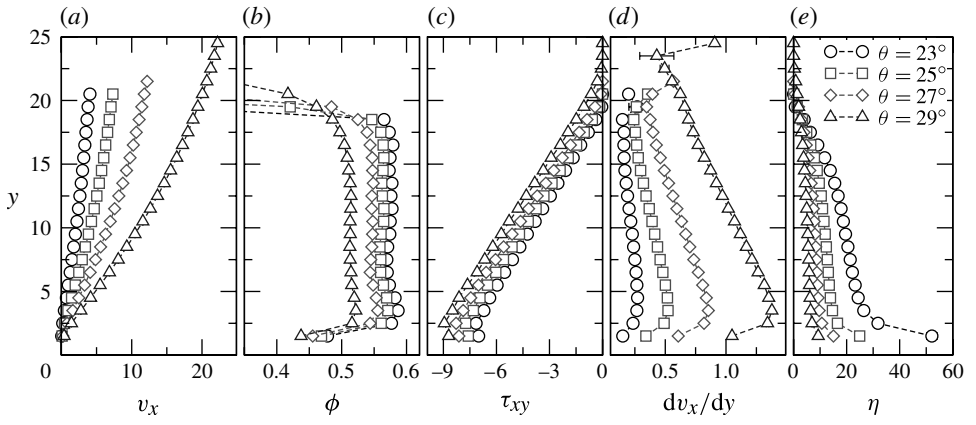

FIGURE 3. (*a*) Velocity, (*b*) solids fraction, (*c*) shear stress, (*d*) shear rate and (*e*) viscosity for light particles flowing in the granular layer at different inclination angles.

ϕ_{max}	ϕ_{max}	I_0	μ_s	μ_m	a
0.59	0.44	0.434	tan(20.16)	tan(37.65)	2/30

TABLE 2. Values of the rheological model parameters (Tripathi & Khakhar 2011*b*).

This completes the formulation of the model for the flow and segregation of a granular mixture of equal-size and different-density particles on a rough inclined plane. All parameters of the model (*b*, and those in table 2) are independently estimated and there are no fitting parameters.

4. Results and discussion

We first present results for the motion of a single heavy particle in flowing light particles (§ 4.1), followed by an analysis of density segregation of mixtures (§ 4.2), in terms of the model given in § 3. Predictions of the flow profiles combining the model for mixture rheology and the model for segregation are presented in § 4.3.

4.1. *Single-particle motion*

Figure 3 shows the flow profiles in the base system: a layer of light particles flowing over an inclined plane for different inclination angles. The results are similar to those reported earlier Tripathi & Khakhar (2011*a*) and are shown here for completeness. The shear rate, $\mathrm{d}v_x/\mathrm{d}y$, is calculated as the numerical derivative of the velocity profile $v_x(y)$ and the viscosity η is calculated as $\eta = |\tau_{xy}|/(\mathrm{d}v_x/\mathrm{d}y)$. The viscosity of the layer increases with depth but the solids volume fraction (ϕ) is nearly constant over most of the depth. Increasing the inclination angle causes an increase in the shear rate and a decrease in the solids fraction and viscosity as shown in figure 3. Thus the inclined plane system serves as a viscous granular fluid, the viscosity of which can be controlled by changing the inclination angle.

The total force acting on a particle due to all the other particles in its vicinity is given in table 3 for different inclination angles for the case of no heavy particles. The

θ (deg.)	$F_b/\cos\theta$	$F_n/\cos\theta$	$F_t/\cos\theta$
23	0.99 ± 0.01	0.97 ± 0.05	0.02 ± 0.04
25	1.04 ± 0.05	1.02 ± 0.07	0.02 ± 0.04
27	1.04 ± 0.06	0.99 ± 0.06	0.05 ± 0.04
29	1.01 ± 0.03	0.98 ± 0.05	0.03 ± 0.02

TABLE 3. Normal (F_n) and tangential (F_t) contributions to the buoyancy force at different inclination angles.

μ_p	$F_b/\cos\theta$	$F_n/\cos\theta$	$F_t/\cos\theta$
0.5	1.04 ± 0.05	1.02 ± 0.07	0.02 ± 0.04
1.0	1.01 ± 0.01	1.00 ± 0.01	0.02 ± 0.01
2.0	1.02 ± 0.02	1.00 ± 0.02	0.02 ± 0.01

TABLE 4. Normal (F_n) and tangential (F_t) contributions to the buoyancy force for different values of friction coefficient μ_p at an inclination of $\theta = 25°$.

force is obtained as a time average of the instantaneous forces acting on the particle, and the computations yield an upward force acting in the y direction, corresponding to the force of buoyancy, F_b. The force (F_b) is well predicted by (3.25) for the different inclination angles, validating the granular buoyancy hypothesis. In the case of fluids, buoyancy is entirely due to pressure. In granular fluids, however, tangential stresses due to frictional forces may also contribute to the buoyancy force. We report the contribution of normal (F_n) and tangential (F_t) forces to the buoyancy force on the light particles for different inclination angles in table 3. As is evident, the tangential force is negligibly small for all the cases and the buoyancy force is entirely due to the normal forces, in the case of granular fluids as well. This indicates symmetry about the xz plane in the y component of the shear stress at the scale of a particle. Table 4 shows the normal and tangential forces on the particles for larger values of the friction coefficient μ_p for a granular layer flowing at an inclination $\theta = 25°$. The contribution of tangential forces to buoyancy is negligible in these cases as well.

We consider next the sedimentation of a single heavy particle in this granular fluid, which is analogous to the Stokes experiment in a fluid. Equation (3.28) suggests a linear variation of ηv with $(m_H - 1)\cos\theta$. We investigate this assumption in figure 4 for different inclination angles ($\theta = 22°$–$29°$) of the layer and different masses of the tracer particle ($m_H = 2$–20). Since the viscosity of the layer is not constant and varies with height y, tracer particles are initiated at four different positions in the layer ($y = 6,\ 10,\ 14$ and 18). The viscosity at any particular inclination angle changes by a factor of 2 for the different positions considered. The linear variation observed in figure 4 at each inclination establishes the validity of (3.7). For lower inclinations ($\theta = 22°$–$23°$), data points are shown only for $y = 10$ and $y = 14$. The data for $y = 6$ and $y = 18$ also show a linear variation but with significantly different slopes and large error bars. At the lower angles, the volume fraction increases and the height of the layer reduces; further, the packing fraction approaches the critical packing fraction for jamming near the base. Boundary effects thus become significant for $y = 6$ and $y = 18$ and these data are omitted.

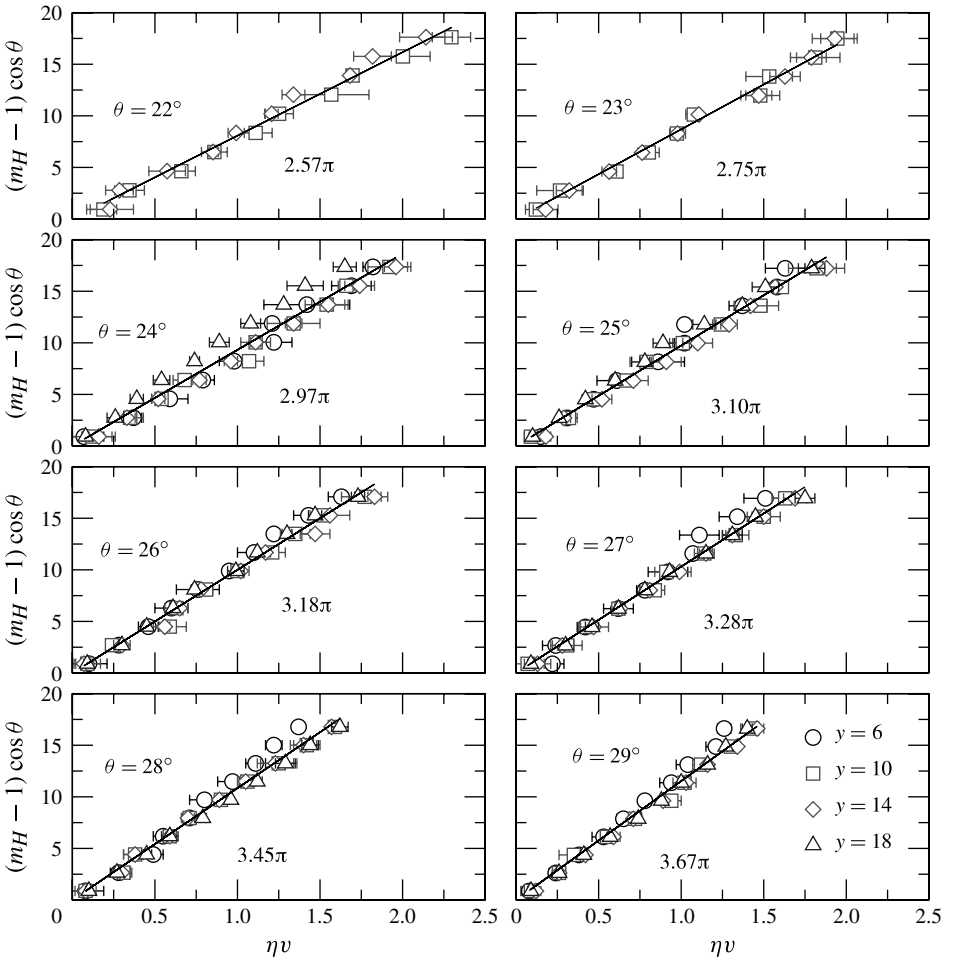

FIGURE 4. Variation of dimensionless drag force on the tracer particle, $(m_H - 1)\cos\theta$, with ηv for different inclinations. Tracer particles of different masses ranging from $m_H = 2$ to $m_H = 20$ are used and the initial depth of the particles (y) is varied. Symbols are the data points, and lines are the fits to the data with their slopes indicated as $c\pi$.

Figure 5 shows the variation of the Stokes law coefficient, c, obtained from the slopes of the fitted lines (figure 4) with solids fraction, ϕ; c decreases with the solids fraction. For the range of packing fractions studied here, the value of c is close to the value observed for a Newtonian fluid, i.e. $c = 3$. The Reynolds number, defined as $Re = \rho_m v/\eta$, for all the cases considered is small and the maximum value of the Reynolds number obtained is $Re = 0.185$. Thus the influence of the inertial forces is small compared to the viscous forces.

4.2. *Segregation of mixtures*

We consider, in this section, a comparison of theoretical predictions of the segregation constitutive equation (3.29) to computational results for mixtures. In the comparison, the values of the viscosity and diffusivity computed from the DEM simulations are used. As a consequence, the segregation model can be tested in isolation, independently of the models for flow and diffusion.

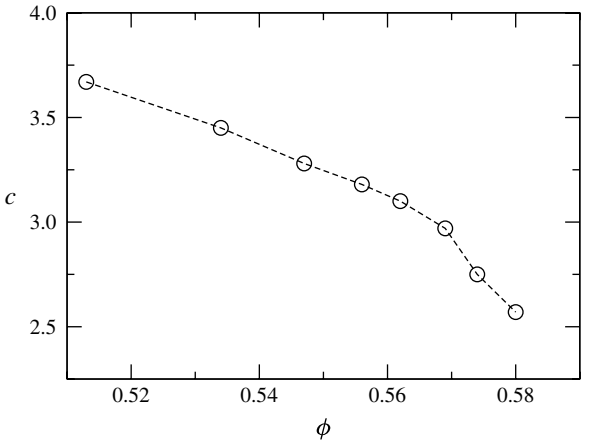

FIGURE 5. Variation of the Stokes law coefficient c (cf. (3.6)) with packing fraction ϕ from the data given in figure 4.

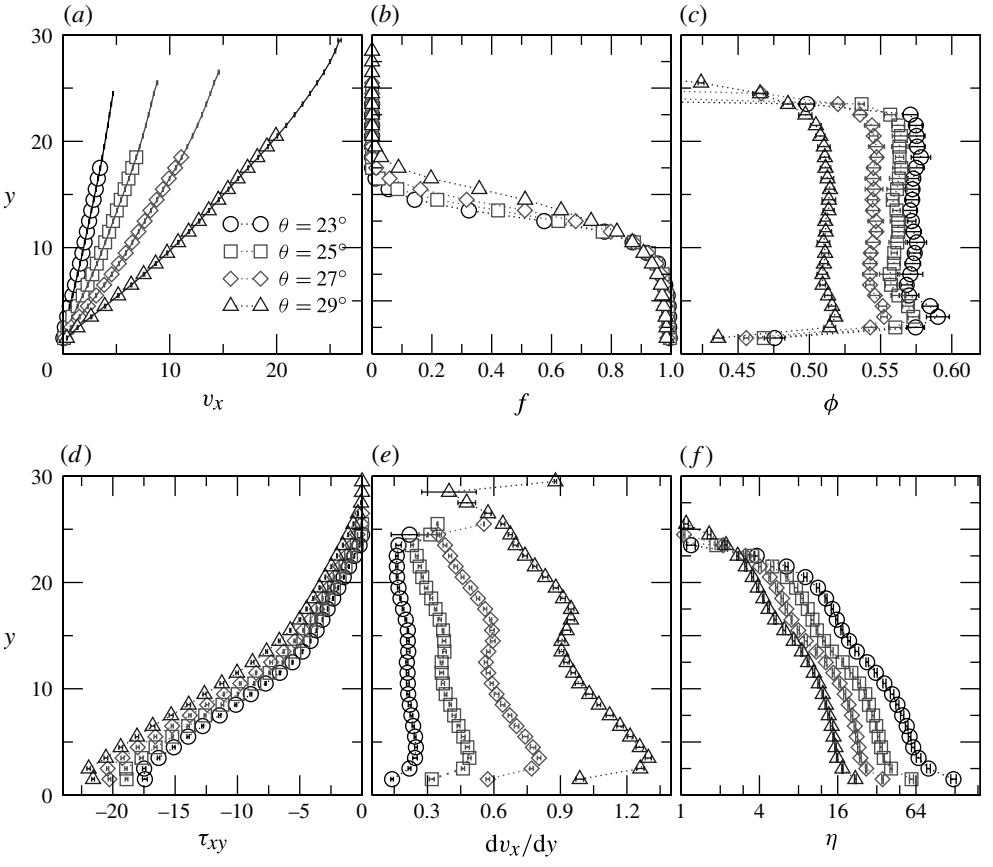

FIGURE 6. (*a*) Velocity, (*b*) number fraction of heavy particles, (*c*) solids fraction, (*d*) shear stress, (*e*) shear rate and (*f*) viscosity of a mixture of 50 % heavy and 50 % light particles (by volume) at different inclination angles for a mass ratio, $m_H = 3$.

Figure 6 shows the velocity (v_x), solids fraction (ϕ) and number fraction of heavy particles (f) of mixtures for different inclination angles for mixtures of 50 % heavy and

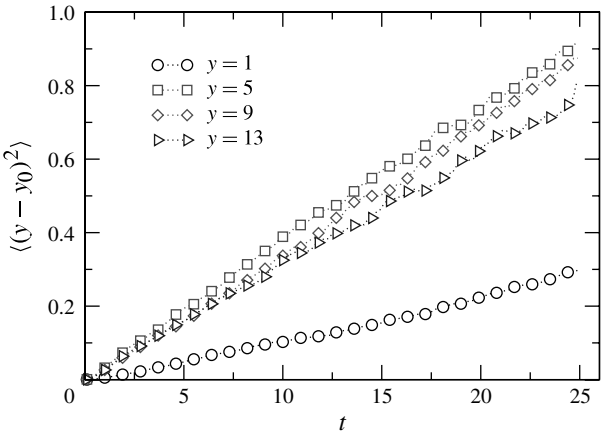

FIGURE 7. Variation of the mean square displacement of heavy particles with time at different y positions in the layer. The results are for a 50 : 50 by volume mixture of heavy and light particles with $m_H = 3$, for an inclination angle $\theta = 25°$.

50 % light particles with mass ratio $m_H = 3$. The results presented are similar to those in Tripathi & Khakhar (2011*b*) and are presented here for completeness. The velocity increases and the solids fraction decreases with the inclination angle. The velocities of the light (lines) and heavy (symbols) particles are equal. The solids fraction ϕ is constant over depth, except near the base and the free surface, as in the case of a pure layer of light particles. Figure 6(*c*) shows that $f = 0$ in the upper part of the layer and $f = 1$ in the lower part of the layer. This indicates complete segregation of the particles, with a pure layer of heavy particles near the base and a pure layer of light particles near the free surface. The thickness of the mixed region increases with the inclination angle, indicating greater mixing for the faster flows. The shear stress (τ_{xy}) shows a linear variation in each of the regions rich in one of the species (figure 6*d*). The slope in the lower region is higher due to the higher bulk density ($\phi\rho_H$) of the pure layer of heavy particles. The shear rate also shows a near linear variation in the pure layers (figure 6*e*) with a sharp reduction in the mixed region due to the sharp increase in the viscosity in that region (figure 6*f*).

Figure 7 shows the variation of mean square displacement $\langle (y - y_0)^2 \rangle$ of the heavy particles with time t for different positions in the layer. The diffusive motion of particles in the y direction is evident by the linear variation of the mean square displacement with time, and the diffusivity is calculated as half of the slope of the line. The diffusivities of the light and heavy particles at any y position are obtained in this manner and are shown in figure 8 for different inclination angles. The diffusivity of the heavy particles (D_H) is equal to that of the light particles (D_L), except at higher inclination angles (lower packing fractions). This again indicates that inertial effects are small. The diffusivity is nearly constant in the upper part of the layer and increases with depth. The reduction in the diffusivity near the base is due to the confining effect of the boundary and has been observed previously as well (Dufresne *et al.* 2000; Lin, Yu & Rice 2000; Tripathi & Khakhar 2010).

Figure 9 shows the variation of the effective temperature with depth in the layer and a comparison of the effective temperature with the kinetic temperature. The effective temperature is calculated as $T_E = c\pi\eta D$, using the values of c obtained from the

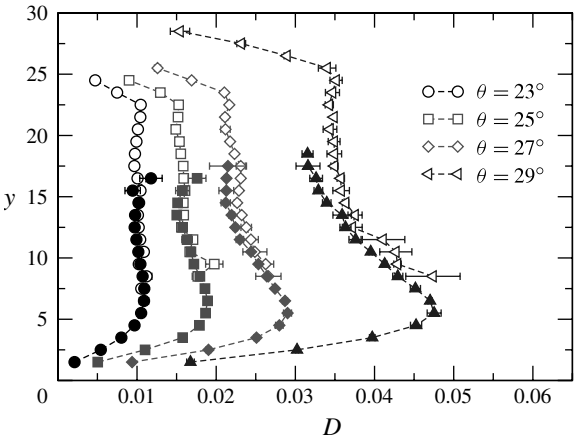

FIGURE 8. Variation of self-diffusivity (D) with depth (y) for a 50 : 50 by volume mixture of heavy and light particles with mass ratio $m_H = 3$ for different inclination angles. Open symbols represent the self-diffusivity of light particles D_L and filled symbols represent the self-diffusivity of heavy particles D_H.

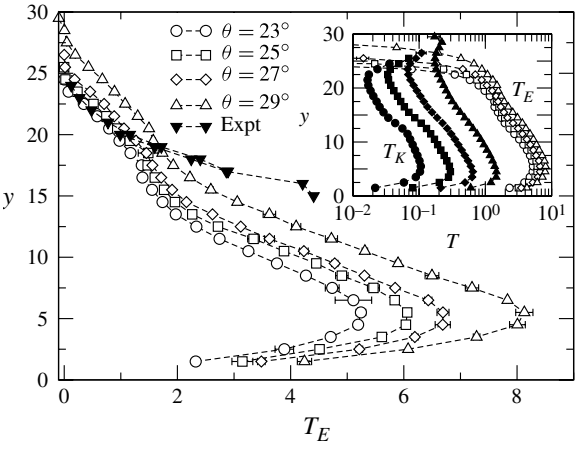

FIGURE 9. Effective temperature profiles ($T_E(y)$) for different inclination angles for a 50 : 50 by volume mixture of heavy and light particles with mass ratio $m_H = 3$. The effective temperature is calculated from $T_E = c\pi\eta D$ using the parameter c from tracer particle studies and the DEM simulation values of η and D for the mixture. The experimental data of Sarkar & Khakhar (2008) (Expt) are also shown for comparison. Inset: comparison of the kinetic granular temperature T_K (filled symbols) and effective temperature T_E.

tracer particle study and the average diffusivity D of the particles, calculated as the weighted mean of the diffusivities, i.e. $D = fD_H + (1-f)D_L$. The variation of effective temperature with height is shown in figure 9 for different inclination angles. The effective temperature of the layer increases with depth and shows a dip near the base (figure 9). The granular temperature, defined as

$$T_K = \tfrac{1}{2}[fm_H u_H^2 + (1-f)m_L u_L^2], \tag{4.1}$$

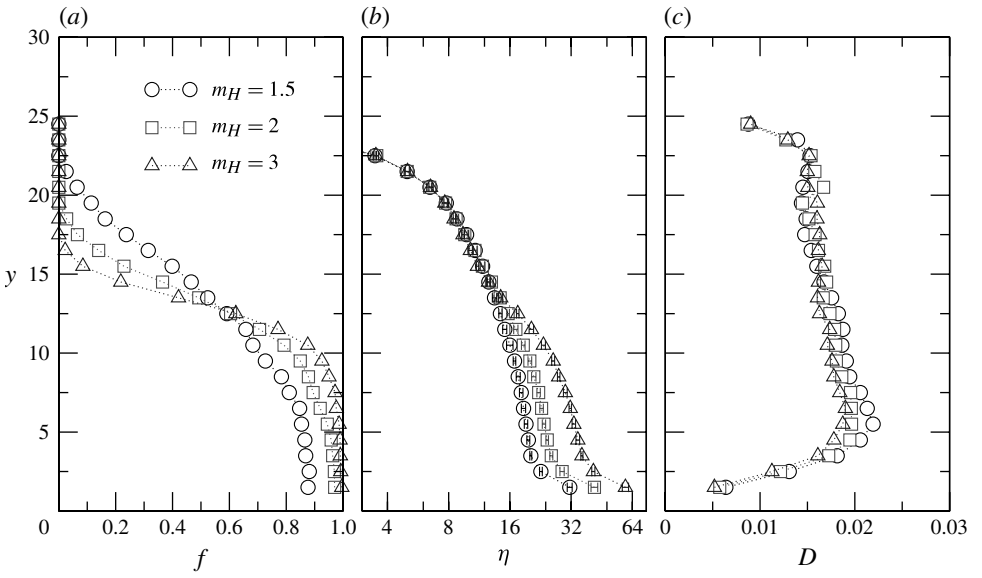

FIGURE 10. (*a*) Number fraction of heavy particles, (*b*) viscosity and (*c*) diffusivity for a mixture of 50 % heavy and 50 % light particles (by volume) at $\theta = 25^\circ$ for different mass ratios (m_H).

where u_H and u_L are the root mean square (r.m.s.) fluctuation velocities of the heavy and light particles, respectively, is compared to the effective temperature in the inset of figure 9. The qualitative behaviour of the effective temperature is the same as that of the granular temperature except near the free surface. The kinetic granular temperature changes by an order of magnitude in the range of the inclination angles considered. The effective temperature, however, changes only by a factor of 2. We further note that the effective temperature T_E is larger than the granular temperature T_K by one to two orders of magnitude. The effective temperature of the layer increases with increasing inclination angle.

The effective temperature obtained experimentally by Sarkar & Khakhar (2008) also shows a similar qualitative behaviour as in the present case. The reduction in the effective temperature near the base, as observed in the present case, however, is absent due to the presence of an erodible base. A comparison of the present data with those of Sarkar & Khakhar (2008) is shown in figure 9. There is good agreement between the two for $T_E < 2$; however, there is a deviation at higher effective temperatures. The differences are due to the different boundary conditions at the base in the two cases.

Figure 10 shows the number fraction, viscosity and diffusivity for different mass ratios $m_H = 1.5$, 2 and 3 of heavy and light particles at a particular inclination angle $\theta = 25^\circ$. The number fraction of the heavy particles f increases near the base and decreases near the free surface with increasing mass ratio. Thus, the segregation of the mixture becomes more pronounced with increasing mass difference, and complete segregation near the free surface and the base is observed for $m_H = 2$ and 3. However, for the smallest mass ratio considered here, the segregation near the base is not complete, and heavy and light particles are partially mixed throughout the layer. The viscosity of the layer increases with the mass ratio owing to the increase in the bulk density. The diffusivity of the particles, however, is almost equal for all the mass ratios considered here. The effective temperature of the mixture increases with increasing

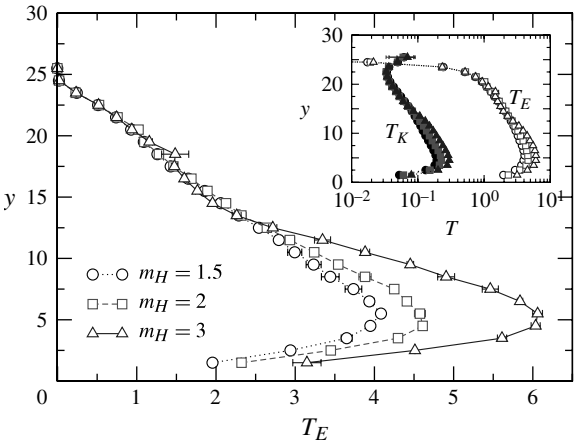

FIGURE 11. Effective temperature profiles ($T_E(y)$) for different mass ratios (m_H) for a 50 : 50 by volume mixture of heavy and light particles for inclination $\theta = 25°$. The effective temperature is calculated from $T_E = c\pi\eta D$ using the parameter c from tracer particle studies and the DEM simulation values of η and D for the mixture. Inset: comparison of the kinetic granular temperature T_K and effective temperature T_E.

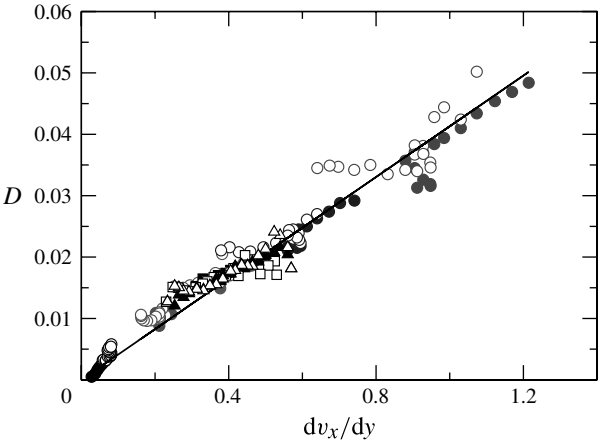

FIGURE 12. Variation of diffusivity with the shear rate $\dot{\gamma} = dv_x/dy$ for a 50 : 50 mixture (by volume) at inclination angle $\theta = 25°$. Open symbols correspond to the self-diffusivity of light particles and filled symbols correspond to the self-diffusivity of heavy particles. Circles denote to mass ratio $m_H = 3$, squares a mass ratio $m_H = 2$, and triangles a mass ratio $m_H = 1.5$. The fitted line has a slope of 0.041.

mass ratio (figure 11) owing to the larger viscosity. As in the previous case, the effective temperature (T_E) is one to two orders of magnitude higher than the kinetic granular temperature (T_K) as shown in figure 11 (inset).

Figure 12 shows the variation of the diffusivity of heavy and light particles with the shear rate. Data near the free surface and the base are omitted. The diffusivity shows a linear variation with the shear rate. Figure 12 shows that the dimensionless diffusivity can be modelled as $D = b\dot{\gamma}$, as noted above (equation (3.31)). A linear least-squares fit to the data (straight line in figure 12) gives $b = 0.041$ from the slope of the fitted line.

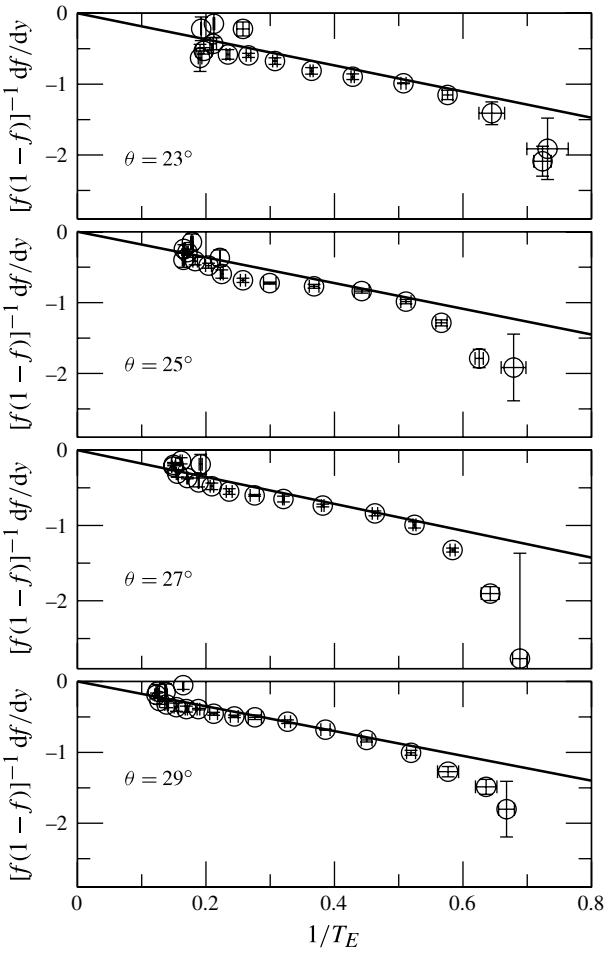

FIGURE 13. Comparison of the theoretical prediction (lines) of density segregation using (3.23) with simulation data (symbols) for different inclination angles for a 50 : 50 mixture (by volume) with mass ratio $m_H = 3$.

The variation of $[f(1-f)]^{-1}\,\mathrm{d}f/\mathrm{d}y$ with $1/T_E$ for different inclination angles θ is shown in figure 13 for a mass ratio $m_H = 3$. Figure 14 shows a similar graph for different mass ratios of heavy and light particles at an inclination angle $\theta = 25°$. The predictions of (3.23) are represented as straight lines and the simulation results are represented with symbols. The theoretical predictions are in good agreement with the simulation results for different inclination angles and for different mass ratios of heavy and light particles. There are no fitted parameters. Deviations from the theoretical predictions are observed in the tail of the data (figures 13 and 14), which corresponds to the region where the number fraction of heavy particles is very small. The comparisons in figures 13 and 14 validate the segregation model.

4.3. *Theoretical prediction of flow profiles using the rheology and segregation models*

We consider next the combined flow and segregation model. An iterative procedure is required for solution of the governing equations, as described below.

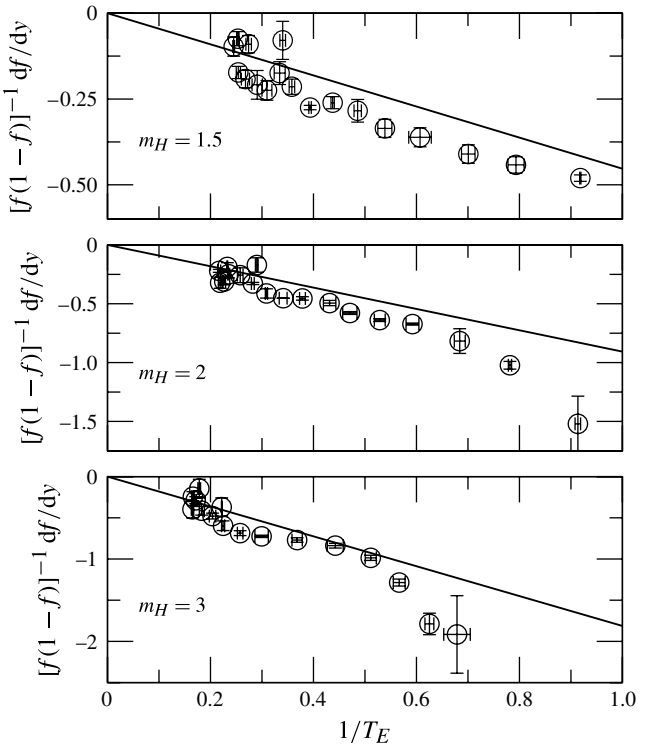

FIGURE 14. Comparison of the theoretical prediction (lines) of density segregation using (3.23) with simulation data (symbols) for different mass ratios for a 50 : 50 mixture (by volume) at inclination angle $\theta = 25°$.

The dimensionless effective temperature can then be written as $T_E = bc\pi|\tau_{xy}|$ using $\eta = |\tau_{xy}|/\dot{\gamma}$ from (3.39) and substituting for D from (3.31). Equation (3.29) thus reduces to

$$\frac{\mathrm{d}f}{\mathrm{d}y}\frac{1}{f(1-f)} = -\frac{(m_H - 1)\cos\theta}{bc\pi|\tau_{xy}|} = -k(y). \tag{4.2}$$

Equation (4.2) is integrated to obtain the number fraction f of heavy particles as

$$f = \frac{\alpha \exp(-\int k(y)\,\mathrm{d}y)}{1 + \alpha \exp(-\int k(y)\,\mathrm{d}y)}, \tag{4.3}$$

where the constant α is obtained using the condition that the total fraction of heavy particles in the mixture (f_T) is specified, i.e.

$$\frac{1}{H}\int_0^H f\,\mathrm{d}y = f_T. \tag{4.4}$$

The inclination angle (θ), the mass ratio of heavy particles (m_H), the total number fraction of heavy particles (f_T) and the depth of the layer (H) are the system parameters, which are the known inputs for the model. In addition, the rheological parameters given in table 2 and $b = 0.041$ are used.

Step 1:	Calculate $\mu(I)$ using (3.40)
Step 2:	Calculate I using (3.41)
Step 3:	Calculate ϕ using (3.34)
Step 4:	Calculate ρ_{mix} using (3.35)
Step 5:	Calculate τ_{xy} and P using (3.32) and (3.33)
Step 6:	Calculate f_{new} using (4.3)
Step 7:	**while** $(\lvert f_{new} - f \rvert > \epsilon_1)$
	$f = f_{new}$
	Repeat Step 4–Step 6
	endwhile
Step 8:	**while** $(\lvert \int_0^H f \, \mathrm{d}y/H - f_T \rvert > \epsilon_2)$
	$\alpha = \alpha + \Delta\alpha$
	Repeat Step 4–Step 7
	endwhile
Step 9:	Calculate $\dot{\gamma}$ using (3.42)
Step 10:	Calculate $v_x(y)$ using (3.43)

TABLE 5. Algorithm for calculating mixture flow properties.

The algorithm for computation of the flow profiles is summarized in table 5. For a given value of α, the profile $f(y)$ is obtained by successive over-relaxation (Step 7 in table 5). The value of α is increased in small increments and the process is repeated until the overall fraction is equal to the specified value (f_T) as given in Step 8. The initial guess for f is taken to be $f(y) = f_T$, i.e. a homogeneous distribution of heavy particles across the layer. The above algorithm is insensitive to the initial guess for $f(y)$ and converges for all the cases provided the increment $\Delta\alpha$ is chosen to be small enough. We use $\alpha = 1$ as the initial guess, increment $\Delta\alpha = 0.1$, and the computational error limits are taken as $\epsilon_1 = 0.001$ and $\epsilon_2 = 0.01$.

The calculated profiles of inertial number I, packing fraction ϕ, number fraction of heavy particles f, shear stress τ_{xy}, shear rate $\dot{\gamma}$ and velocity $v_x(y)$ are shown in figure 15 for different inclination angles for 50 % heavy particle ($m_H = 3$) mixture. Figures 16 and 17 show the flow profiles for different mass ratios and different compositions of the mixture. The theoretical predictions match very well with the simulation results for all the cases. The complex nature of the shear rate for different compositions and mass ratios is well captured by the theory and is in good agreement with the simulation results. Note also that the extent of segregation of the heavy particles $f(y)$ for all the cases is very well described by the theory.

5. Conclusions

We presented a detailed study of granular segregation in binary mixtures of equal-size particles of different density, in a dense gravity-driven flow on a rough inclined plane. Results of numerical simulations using DEM for the motion of a single high-density particle in the flow were analysed using a continuum theory. The buoyancy force was found to be given by Archimedes principle, with the effective volume of the particle, which takes into account excluded-volume effects, given by $V_E = V/\phi$. The drag force was found to be given by a modified Stokes law ($F_d = c\pi\eta v d$), with the coefficient (c) reducing with increasing solids volume fraction (ϕ). The buoyancy force on the particle was shown to be primarily due to normal forces, with a negligible contribution from tangential forces.

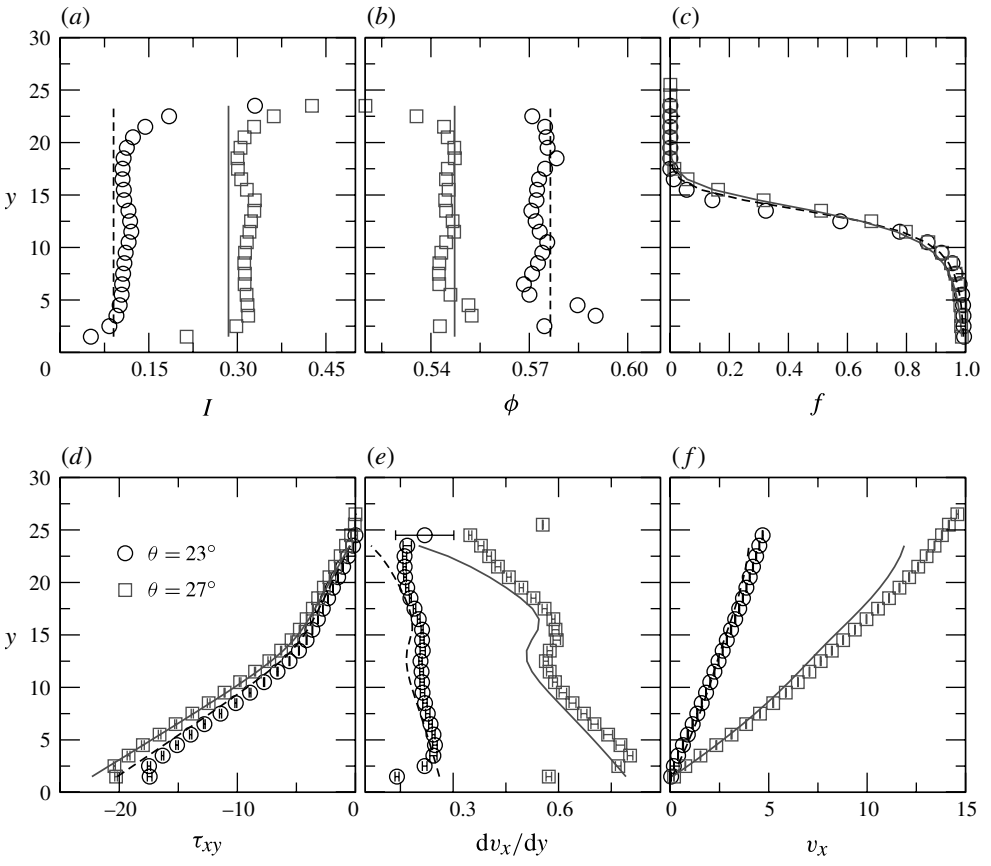

FIGURE 15. Comparison of the theoretical prediction (lines) with simulation results (symbols) for different inclination angles of 50 % heavy ($m_H = 3$) particle mixtures.

DEM results were presented for binary mixtures for equal-diameter and different-mass particles flowing on a rough inclined plane for different inclination angles, concentrations and mass ratios. In all cases, the system exhibited significant segregation, with heavy particles sinking into the lower region of the layer and the light particles rising into the upper region, with a mixed interface region in between. The mean velocities of the heavy and light particles in the mixture at any given depth were found to be equal and there was no slip between the species. The self-diffusivities of the heavy and light particles at any given depth were also found to be equal to each other and thus the same as the binary diffusivity. The diffusivities were found to vary linearly with shear rate.

With increase in inclination angle, the packing fraction reduced from $\phi = 0.58$ to $\phi = 0.5$, resulting in an increase in the mean velocity and diffusivity but a decrease in the viscosity. The thickness of the mixed zone increased with angle. Increasing the mass ratio did not affect the packing fraction of the layer and the diffusivity of the particles. However, the extent of segregation increased with increasing mass ratio, leading to nearly complete segregation of light particles near the free surface and complete segregation of heavy particles near the base for $m_H > 2$. The effective temperature increased with the inclination angle and the mass ratio of the particles and

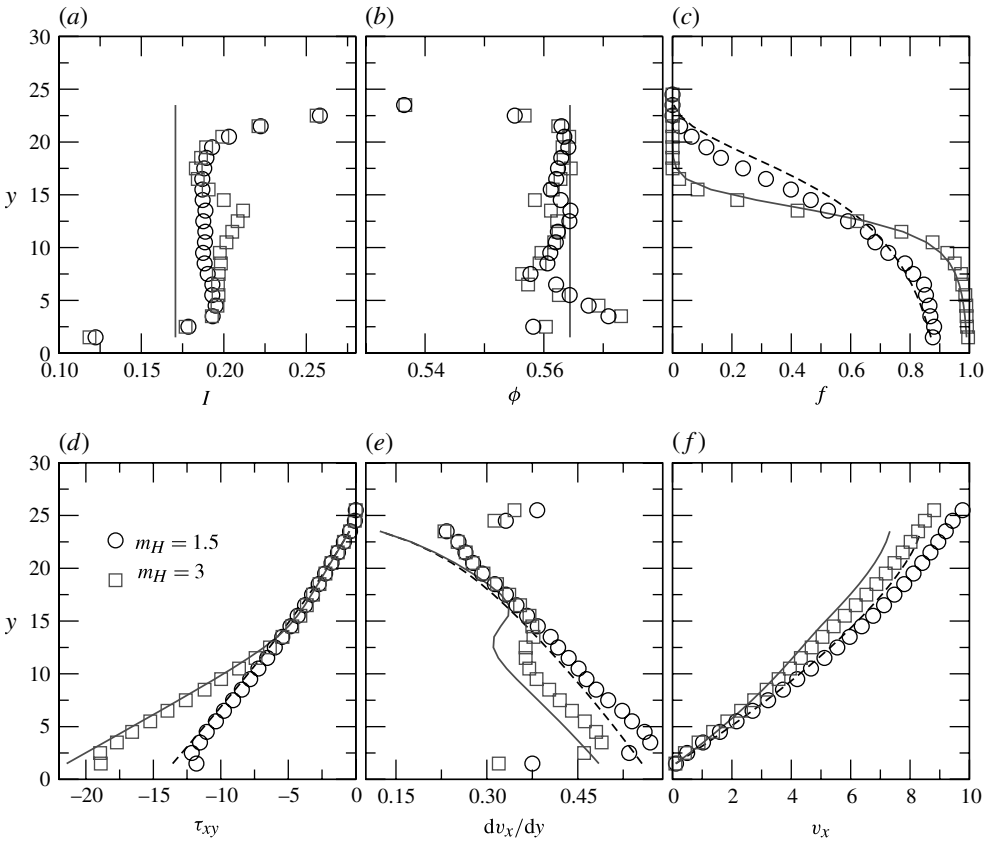

FIGURE 16. Comparison of the theoretical prediction (lines) with simulation results (symbols) for 50 % heavy particle mixture for different mass ratios (m_H) at an inclination $\theta = 25°$.

was at least an order of magnitude higher than the kinetic granular temperature. The computed effective temperatures were in reasonable agreement with the measurements of Sarkar & Khakhar (2008).

Based on the single-particle results and following Sarkar & Khakhar (2008), a theory was presented for the segregation of such mixtures. The theory predicts the equilibrium number fraction profile in terms of the effective temperature, which in turn depends on the local viscosity and self-diffusivity of the particles. The theory gave good predictions of the equilibrium number fraction profiles, using the computed viscosity and self-diffusivity as inputs. Finally, the segregation model was combined with the rheological model given by Tripathi & Khakhar (2011*b*) and an empirical expression for the self-diffusivity to yield profiles of inertial number, volume fraction, number fraction, shear stress, shear rate and mean velocity in the layer. The flow and segregation processes are coupled and the profiles were computed using an iterative procedure. The predicted profiles match with the simulation results for the different cases studied.

The results indicate that the relatively simple continuum model yields a detailed and accurate description of the flow and segregation in the case of mixtures of equal-size and different-density particles. The components of the model are individually validated

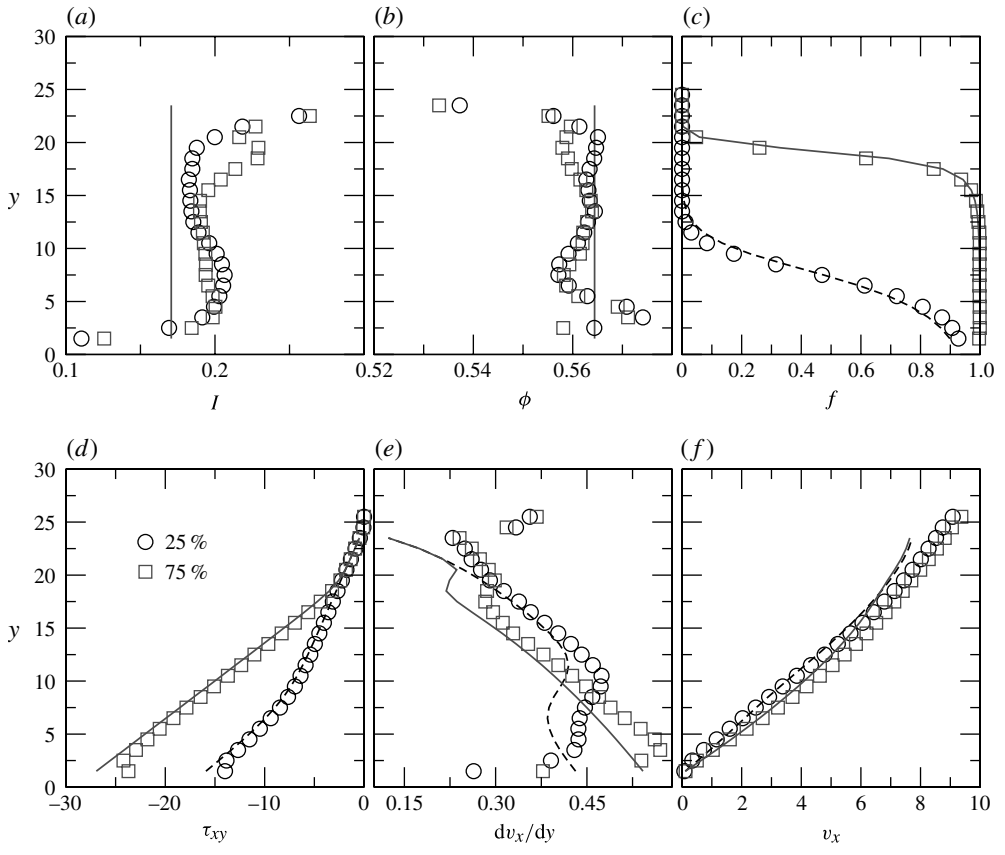

FIGURE 17. Comparison of the theoretical prediction (lines) with simulation results (symbols) for different volume fractions of heavy particle ($m_H = 3$) mixtures at an inclination $\theta = 25°$.

by DEM simulations in three stages: (i) single-particle motion; (ii) segregation model alone; and (iii) combined models for flow, segregation and diffusion. A natural extension of the approach would be to consider different-size particles. This, however, introduces two complexities: firstly, the effective volume, used for estimation of the buoyancy force, is different for the different-size particles and is not straightforward to estimate; secondly, the binary diffusivity is required for the diffusion flux, which is different from the self-diffusivity. We will report these results separately.

REFERENCES

ALBERT, R., PFEIFER, M. A., BARABÁSI, A.-L. & SCHIFFER, P. 1999 Slow drag in a granular medium. *Phys. Rev. Lett.* **82** (1), 205–208.

BARRAT, J. L. & BERTHIER, L. 2000 Fluctuation–dissipation relation in a sheared fluid. *Phys. Rev.* E **63** (1), 012503.

BERTHIER, L. & BARRAT, J. L. 2002 Shearing a glassy material: numerical tests of nonequilibrium mode-coupling approaches and experimental proposals. *Phys. Rev. Lett.* **89**, 095702.

BERTHIER, L., BARRAT, J. L. & KURCHAN, J. 2000 A two-time scale, two-temperature scenario for nonlinear rheology. *Phys. Rev.* E **61**, 5464.

BRITO, R., ENRIQUEZ, H., GODOY, S. & SOTO, R. 2008 Segregation induced by inelasticity in a vibrofluidized granular mixture. *Phys. Rev.* E **77** (6), 061301.

BRITO, R. & SOTO, R. 2009 Competition of brazil nut effect, buoyancy, and inelasticity induced segregation in a granular mixture. *Eur. Phys. J. Special Topics* **179**, 207–219.

CABALLERO-ROBLEDO, G. A. & CLEMENT, E. 2009 Rheology of a sonofluidized granular packing. *Eur. Phys. J.* E **30**, 395–401.

CANDELIER, R. & DAUCHOT, O. 2009 Creep motion of an intruder within a granular glass close to jamming. *Phys. Rev. Lett.* **103** (12), 128001.

CANDELIER, R. & DAUCHOT, O. 2010 Journey of an intruder through the fluidization and jamming transitions of a dense granular media. *Phys. Rev.* E **81** (1), 011304.

CHEHATA, D., ZENIT, R. & WASSGREN, C. R. 2003 Dense granular flow around an immersed cylinder. *Phys. Fluids* **15**, 1622.

CHUNG, F., LIAW, S.-S. & JU, C.-Y. 2009 Brazil nut effect in a rectangular plate under horizontal vibration. *Granul. Matt.* **11**, 79–86.

CISAR, S. E., UMBANHOWAR, P. B. & OTTINO, J. M. 2006 Radial granular segregation under chaotic flow in two-dimensional tumblers. *Phys. Rev.* E **74** (5), 051305.

COSTANTINO, D. J., BARTELL, J., SCHEIDLER, K. & SCHIFFER, P. 2011 Low-velocity granular drag in reduced gravity. *Phys. Rev.* E **83** (1), 011305.

DOLGUNIN, V. N., KUDY, A. N. & UKOLOV, A. A. 1998 Development of the model of segregation of particles undergoing granular flow down an inclined plane. *Powder Technol.* **96**, 211–218.

DOLGUNIN, V. N. & UKOLOV, A. A. 1995 Segregation modelling of particle rapid gravity flow. *Powder Technol.* **83**, 95–103.

DRAHUN, J. A. & BRIDGWATER, J. 1983 Mechanisms of free surface segregation. *Powder Technol.* **36**, 39–53.

DUFRESNE, E. R., SQUIRES, T. M., BRENNER, M. P. & GRIER, D. G. 2000 Hydrodynamic coupling of two Brownian spheres to a planar surface. *Phys. Rev. Lett.* **85** (15), 3317–3320.

DURAN, J. 2000 *Sands, Powders, and Grains: An Introduction to the Physics of Granular Materials*. Springer.

FELIX, G. & THOMAS, N. 2004 Evidence of two effects in the size segregation process in dry granular media. *Phys. Rev.* E **70**, 051307.

GENG, J. & BEHRINGER, R. P. 2005 Slow drag in two-dimensional granular media. *Phys. Rev.* E **71** (1), 011302.

GODOY, S., RISSO, D., SOTO, R. & CORDERO, P. 2008 Rise of a brazil nut: a transition line. *Phys. Rev.* E **78** (3), 031301.

GRAY, J. M. N. T. & CHUGUNOV, V. A. 2006 Particle-size segregation and diffusive remixing in shallow granular avalanches. *J. Fluid Mech.* **569**, 365–398.

GRAY, J. M. N. T. & THORNTON, A. R. 2005 A theory for particle size segregation in shallow granular free-surface flows. *Proc. R. Soc.* A **461**, 1447–1473.

HAJRA, S. K. & KHAKHAR, D. V. 2005 Radial mixing of granular materials in a rotating cylinder: experimental determination of particle self-diffusivity. *Phys. Fluids* **17**, 013101.

HAJRA, S. K. & KHAKHAR, D. V. 2011 Radial segregation of ternary granular mixtures in rotating cylinders. *Granul. Matt.* **13**, 475–486.

HILL, K. M., KHAKHAR, D. V., GILCHRIST, J. F., MCCARTHY, J. J. & OTTINO, J. M. 1999 Segregation-driven organization in chaotic granular flows. *Proc. Natl Acad. Sci. USA* **96** (21), 11701–11706.

HIRSHFELD, D. & RAPAPORT, D. C. 1997 Molecular dynamics studies of grain segregation in sheared flow. *Phys. Rev.* E **56** (2), 2012–2018.

HSIAU, S. S. & CHEN, W. C. 2002 Density effect of binary mixtures on the segregation process in a vertical shaker. *Adv. Powder Technol.* **13** (3), 301–315.

JAIN, N., OTTINO, J. M. & LUEPTOW, R. M. 2005 Regimes of segregation and mixing in combined size and density granular systems: an experimental study. *Granul. Matt.* **7**, 69–81.

JENKINS, J. T. & MANCINI, F. 1989 Kinetic theory for binary mixtures of smooth, nearly elastic, spheres. *Phys. Fluids* A **1**, 2050–2057.

JOHNSON, C. G., KOKELAAR, B. P., IVERSON, R. M., LOGAN, M., LAHUSEN, R. G. & GRAY, J. M. N. T. 2012 Grain-size segregation and levee formation in geophysical mass flows. *J. Geophys. Res. Earth Surf.* **117**, F01032.

JOP, P., FORTERRE, Y. & POULIQUEN, O. 2006 A new constitutive law for dense granular flows. *Nature* **441**, 727–730.

KHAKHAR, D. V., MCCARTHY, J. J. & OTTINO, J. M. 1997 Radial segregation of granular materials in a rotating cylinder. *Phys. Fluids* **9** (12), 3600–3614.

KHAKHAR, D. V., MCCARTHY, J. J. & OTTINO, J. M. 1999 Mixing and segregation of granular materials in chute flows. *Chaos* **9**, 594–610.

KHAKHAR, D. V., ORPE, A. V. & HAJRA, S. K. 2003 Segregation of granular materials in rotating cylinders. *Physica* A **318** (1–2), 129–136.

KURCHAN, J. 2000 Emergence of macroscopic temperatures in systems that are not thermodynamical microscopically: towards a thermodynamical description of slow granular rheology. *J. Phys.: Condens. Matter* **12**, 6611.

LIM, E. W. C. 2010 Density segregation in vibrated granular beds with bumpy surfaces. *AIChE J.* **56**, 2588–2597.

LIN, B., YU, J. & RICE, S. A. 2000 Direct measurements of constrained Brownian motion of an isolated sphere between two walls. *Phys. Rev.* E **62** (3), 3909–3919.

LINARES-GUERRERO, E., GOUJON, C. & ZENIT, R. 2007 Increased mobility of bidisperse granular avalanches. *J. Fluid Mech.* **593**, 475–504.

MAKSE, H. A. & KURCHAN, J. 2002 Testing the thermodynamic approach to granular matter with a numerical model of a decisive experiment. *Nature* **415**, 614.

MARKS, B., ROGNON, P. & EINAV, I. 2012 Grainsize dynamics of polydisperse granular segregation down inclined planes. *J. Fluid Mech.* **690**, 499–511.

MEHTA, A. & EDWARDS, S. F. 1989 Statistical mechanics of powder mixtures. *Physica* A **157**, 1091.

OTTINO, J. M. & KHAKHAR, D. V. 2000 Mixing and segregation of granular materials. *Annu. Rev. Fluid Mech.* **32**, 55–91.

PEREIRA, G., SINNOTT, M., CLEARY, P., LIFFMAN, K., METCALFE, G. & ŠTALO, I. 2011 Insights from simulations into mechanisms for density segregation of granular mixtures in rotating cylinders. *Granul. Matt.* **13**, 53–74.

PHILLIPS, J. C., HOGG, A. J., KERSWELL, R. R. & THOMAS, N. H. 2006 Enhanced mobility of granular mixtures of fine and coarse particles. *Earth Planet. Sci. Lett.* **246**, 466–480.

PICA CIAMARRA, M., LARA, A. H., LEE, A. T., GOLDMAN, D. I., VISHIK, I. & SWINNEY, H. L. 2004 Dynamics of drag and force distributions for projectile impact in a granular medium. *Phys. Rev. Lett.* **92** (19), 194301.

POLLARD, B. L. & HENEIN, H. 1989 Kinetics of radial segregation of different sized irregular particles in rotary cylinders. *Can. Metall. Q.* **28** (1), 29–40.

RAPAPORT, D. C. 2002 Simulational studies of axial granular segregation in a rotating cylinder. *Phys. Rev.* E **65**, 061306.

RISTOW, G. H. 1994 Particle mass segregation in a two-dimensional rotating drum. *Europhys. Lett.* **28**, 97–101.

SANFRATELLO, L. & FUKUSHIMA, E. 2008 Experimental studies of density segregation in the 3D rotating cylinder and the absence of banding. *Granul. Matt.* **11** (2), 73–78.

SARKAR, S. & KHAKHAR, D. V. 2008 Experimental evidence for a description of granular segregation in terms of the effective temperature. *Europhys. Lett.* **83** (5), 54004.

SAVAGE, S. B. 1993 Disorder, diffusion and structure formation in granular flow. In *Disorder and Granular Media* (ed. A. Hansen & D. Bideau), pp. 255–285. Elsevier.

SAVAGE, S. B. & LUN, C. K. K. 1988 Particle size segregation in inclined chute flow of dry cohesionless granular solids. *J. Fluid Mech.* **189**, 311–335.

SCHRÖTER, M., ULRICH, S., KREFT, J., SWIFT, J. B. & SWINNEY, H. L. 2006 Mechanisms in the size segregation of a binary granular mixture. *Phys. Rev.* E **74** (1), 011307.

SHI, Q., SUN, G., HOU, M. & LU, K. 2007 Density-driven segregation in vertically vibrated binary granular mixtures. *Phys. Rev.* E **75**, 061302.

SILBERT, L. E., ERTAS, D., GREST, G. S., HASLEY, T. C., LEVINE, D. & PLIMPTON, S. J. 2001 Granular flow down an inclined plane: Bagnold scaling and rheology. *Phys. Rev.* E **64**, 051302.

SONG, C., WANG, P. & MAKSE, H. A. 2005 Experimental measurement of an effective temperature for jammed granular materials. *Proc. Natl Acad. Sci. USA* **102**, 2299.

SREBRO, Y. & LEVINE, D. 2003 Role of friction in compaction and segregation of granular materials. *Phys. Rev.* E **68** (6), 061301.

TAI, C. H., HSIAU, S. S. & KRUELLE, C. A. 2010 Density segregation in a vertically vibrated granular bed. *Powder Technol.* **204** (2–3), 255–262.

TAKEHARA, Y., FUJIMOTO, S. & OKUMURA, K. 2010 High-velocity drag friction in dense granular media. *Europhys. Lett.* **92**, 44003.

THOMAS, N. 2000 Reverse and intermediate segregation of large beads in dry granular media. *Phys. Rev.* E **62** (1), 961–974.

TRIPATHI, A. & KHAKHAR, D. V. 2010 Steady flow of smooth, inelastic particles on a bumpy inclined plane: hard and soft particle simulations. *Phys. Rev.* E **81** (4), 041307.

TRIPATHI, A. & KHAKHAR, D. V. 2011*a* Numerical simulation of the sedimentation of a sphere in a sheared granular fluid: a granular Stokes experiment. *Phys. Rev. Lett.* **107**, 108001.

TRIPATHI, A. & KHAKHAR, D. V. 2011*b* Rheology of binary granular mixtures in the dense flow regime. *Phys. Fluids* **23** (11), 113302.

ULRICH, S., SCHRÖTER, M. & SWINNEY, H. L. 2007 Influence of friction on granular segregation. *Phys. Rev.* E **76** (4), 042301.

WASSGREN, C. R., CORDOVA, J. A., ZENIT, R. & KARION, A. 2003 Dilute granular flow around an immersed cylinder. *Phys. Fluids* **15**, 3318.

WIEDERSEINER, S., ANDREINI, N., EPELY-CHAUVIN, G., MOSER, G., MONNEREAU, M., GRAY, J. M. N. T. & ANCEY, C. 2011 Experimental investigation into segregating granular flows down chutes. *Phys. Fluids* **23** (1)013301.

WIEGHARDT, K. 1975 Experiments in granular flow. *Annu. Rev. Fluid Mech.* **7**, 89–114.

YANG, S. C. 2006 Density effect on mixing and segregation processes in a vibrated granular mixture. *Powder Technol.* **164**, 65–74.

ZHOU, F., ADVANI, S. G. & WETZEL, E. D. 2004 Slow drag in granular materials under high pressure. *Phys. Rev.* E **69** (6), 061306.

ZHOU, F., ADVANI, S. G. & WETZEL, E. D. 2005 Slow drag in polydisperse granular mixtures under high pressure. *Phys. Rev.* E **71** (6), 061304.

ZHOU, F., ADVANI, S. G. & WETZEL, E. D. 2007 Simulation of slowly dragging a cylinder through a confined pressurized bed of granular materials using the discrete element method. *Phys. Fluids* **19**, 013301.

ZIK, O., STAVANS, J. & RABIN, Y. 1992 Mobility of a sphere in vibrated granular media. *Europhys. Lett.* **17** (4), 315.